Available online at www.sciencedirect.com
SCIENCE DIRECT
Journal of Power Sources 158 (2006) 213–224
JOURNAL OF POWER SOURCES
www.elsevier.com/locate/jpowsour

Analysis of a molten carbonate fuel cell: Numerical modeling and experimental validation

Jacob Brouwer [a,*], Faryar Jabbari [b], Elisângela Martins Leal [b], Trevor Orr [b]

[a] *National Fuel Cell Research Center, University of California, Irvine, CA 92697, USA*
[b] *Department of Mechanical and Aerospace Engineering, University of California, Irvine, CA 92697, USA*

Received 5 July 2005; accepted 30 July 2005
Available online 14 November 2005

Abstract

A detailed dynamic model incorporating geometric resolution of a molten carbonate fuel cell (MCFC) with dynamic simulation of physical and electrochemical processes in the stream-wise direction is presented. The model was developed using mass and momentum conservation, electrochemical and chemical reaction mechanisms, and heat-transfer. Results from the model are compared with data from an experimental MCFC unit. Furthermore, the model was applied to predict dynamic variations of voltage, current and temperature in an MCFC as it responds to varying load demands. The voltage was evaluated using two different approaches: one applying a model developed by Yuh and Selman [C.Y. Yuh, J.R. Selman, The polarization of molten carbonate fuel cell electrodes: I. Analysis of steady-state polarization data, J. Electrochem. Soc. 138 (1991) 3642–3648; C.Y. Yuh, J.R. Selman, The polarization of molten carbonate fuel cell electrodes: II. Characterization by AC impedance and response to current interruption, J. Electrochem. Soc. 138 (1991) 3649–3655] and another applying simplified equations using average local temperatures and pressures. The results show that both models can be used to predict voltage and dynamic response characteristics of an MCFC and the model that uses the more detailed Yuh and Selman approach can predict those accurately and consistently for a variety of operating conditions.

Keywords: Molten carbonate fuel cell; Agglomerate model; Generalized model; Heat transfer; Experimental analysis

1. Introduction and background

The development of energy systems with readily available fuels, high efficiency and minimal environmental impact are required in order to meet increasing energy demands and to respond to environmental concerns. Increasingly, fuel cell systems are being considered as promising solutions. Fuel cell-based power plants convert the chemical energy in a fuel directly to electricity without the need to first convert chemical energy into heat. This results in high efficiency and low pollutant emissions in comparison to traditional fossil fuel-based energy conversion devices.

Among the various fuel cell types, the molten carbonate fuel cell (MCFC) is a very promising technology, which is now commercially available. It has been mainly applied for stationary generation of electrical energy together with the production of highly valuable heat and is thus suitable for many industrial applications as well as for distributed power supply. Molten carbonate fuel cells normally operate at approximately 650 °C. This operating temperature is needed to achieve sufficient ionic conductivity in its electrolyte. High temperature operation is also advantageous for the system in terms of the production of high quality waste heat and fuel flexibility (i.e., ability to electrochemically oxidize carbon monoxide and hydrocarbon fuels and to reform hydrocarbon fuels within the fuel cell stack). In addition, typical MCFC operating temperatures produce sufficiently fast electrochemical kinetics that noble metal catalysts are not required for the cell electrochemical oxidation and reduction processes. On the other hand, degradation of cell materials and other system components is negatively impacted by the higher operating temperatures and especially by thermal cycling.

The molten carbonate fuel cell uses a carbonate electrolyte, which is generally a mixture of lithium and potassium carbonates (salts). The electrolyte materials, which become molten

* Corresponding author. Tel.: +1 949 824 1999x221.
E-mail addresses: jb@nfcrc.uci.edu (J. Brouwer), fjabbari@eng.uci.edu (F. Jabbari), eleal@uci.edu (E.M. Leal).

0378-7753/$ – see front matter © 2005 Elsevier B.V. All rights reserved.
doi:10.1016/j.jpowsour.2005.07.093

Nomenclature

A	Area of the cell (m^2)
A_{cond}	Flux area of the solid (m^2)
A_{conv}	Exposed surface area of the solid (m^2)
C_k	Individual concentration of specie k ($mol\,m^{-3}$)
E	Energy (J)
E_1	Net rate of flow energy added at control volume inlet and outlet. Zero for exit control volume where enthalpy is directly used in the conservation equation (W)
E_0	Ideal standard potential (V)
E_{act}	Activation energy ($J\,mol^{-1}$)
E_{eq}	Nernst potential (V)
E_{in}	Energy into control volume ($J\,g^{-1}$)
E_{out}	Energy out of control volume ($J\,g^{-1}$)
F	Faraday's constant (96,487 $C\,mol^{-1}$)
h	Convective heat transfer coefficient
$\Delta H^f_{H_2O}$	Heat of formation of water ($W\,m^{-2}\,K^{-1}$)
j	Current generated (A)
j_0	Exchange current density ($A\,m^{-2}$)
j_L	Limiting current density ($A\,m^{-2}$)
k	Thermal conductivity ($W\,m^{-1}\,K^{-1}$)
L	Distance between the bulk temperature (m)
m_{in}	Mass flux into control volume ($g\,s^{-1}$)
m_{out}	Mass flux out of control volume ($g\,s^{-1}$)
n	Number of participating electrons in the reaction (–)
N_k	Molar flow of specie k ($mol\,s^{-1}$)
p_k	Partial pressure of specie k (Pa)
P	Pressure (Pa)
Q_{ref}	Reformer heat exchange losses (W)
Q_{conv}	Convective heat transfer (W)
Q_{cond}	Conductive heat transfer (W)
R_{int}	Internal resistance of the fuel cell ($\Omega\,m^2$)
R_{load}	Total load resistance (Ω)
R_{ohm}	Ohmic resistance (Ω)
R_p	Total production rate of species k ($mol\,s^{-1}$)
R_u	Universal gas constant ($8.3145\,J\,mol^{-1}\,K^{-1}$)
t	Time (s)
T	Temperature (K)
$\forbar{V}$	Finite control volume (m^3)
V_{cell}	Cell voltage (V)

Greek letters

α	Transfer coefficient (–)
η_{act}	Activation polarization (V)
η_{an}	Impedance for anode overpotential (Ω)
η_{cat}	Impedance for cathode overpotential (Ω)
η_{conc}	Concentration polarization (V)
η_{ohm}	Ohmic polarization (V)
ρ	Density ($g\,m^{-3}$)

Superscripts

an	anode
cat	cathode
cs	cathode side
ele	electrolyte
s	separator plate

at typical operating temperatures, are usually supported and wicked to cover electrode surfaces through use of a ceramic electrolyte support mesh (often $LiAlO_2$). Anode materials are typically Ni–Cr/Ni–Al alloys and cathode materials are comprised of lithiated NiO. The fuel cell operation is the result of a complex conjunction of physical, chemical and electrochemical processes. The anode and cathode half reactions and overall electrochemical reaction are [3]:

$$\text{Cathode}: \quad 0.5O_2 + CO_2 + 2e^- \rightarrow {CO_3}^{2-} \tag{1}$$

$$\text{Anode}: \quad H_2 + CO_3^{2-} \rightarrow H_2O + CO_2 + 2e^- \tag{2}$$

$$\text{Overall}: \quad H_2 + 0.5O_2 + CO_{2,cat} \rightarrow H_2O + CO_{2,an} + \text{electricity} + \text{heat}_{stack} \tag{3}$$

Several groups have investigated and advanced MCFC technology over the years. These groups include the Illinois Institute of Technology, Delft University, the Gas Technology Institute (formerly GRI), Ansaldo Ricerche, CRIEPI, and others [4]. The most significant advancements and recent investments in MCFC technology have been from the governments of the United States and Japan and from FuelCell Energy Corporation (formerly Energy Research Corporation) of the U.S., Mitsubishi Heavy Industries (MHI) of Japan, and MTU of Germany. Molten carbonate fuel cell power plants of 250 kW, 1.5 MW, and 3.0 MW are currently commercially available [5].

2. Model formulation

The molten carbonate fuel cell (MCFC) studied here is presented schematically in Fig. 1. The cell has a planar configuration with co-flow channel flows. It can be physically broken down into 5 distinct components: anode and cathode separator plates, electrode–electrolyte assembly, and anode and cathode gas channels. The separator plates are used to provide structural support to the electrolyte mesh as well as to separate the anode and cathode channels. The electrode–electrolyte assembly is where chemical reactions occur and current and heat are generated. Although this assembly is a complicated molten structure with certain concentration of carbonate ions traveling through and chemical reactions at interfaces on both sides, it was modeled as a solid structure with electrochemistry and ion transport sufficiently fast to allow the assumption of no mass storage. The mass of the electrolyte accounts for the presence of ions and the reduction and oxidation reactions are assumed to happen at the surface of this solid assembly. The gas channel flows are where the products and reactants are brought to and from the electrode–electrolyte surface. In the gas channels of the model, all of the dynamic conservation equations (mass,

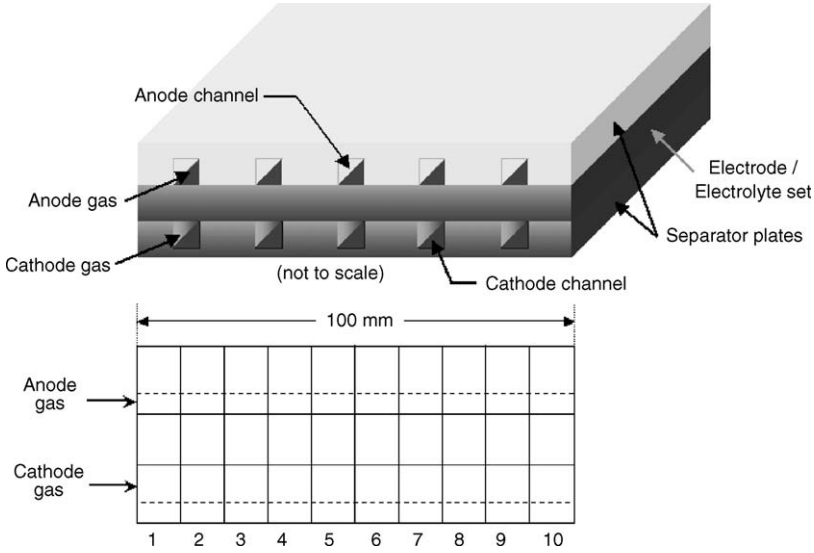

Fig. 1. Schematic showing the geometry of the molten carbonate fuel cell dynamic model [13].

species, momentum, and energy) are solved simultaneously. The simplified geometry that is included in the model breaks the cell into 10 equidistant nodes along the length of the cell as shown in Fig. 1. Each node includes resolution of the 5 cell components described above. Previous nodal sensitivity studies [6] have shown that 10 nodes are sufficient to capture the performance of an MCFC cell of the current size and shape.

The electrochemistry in the cell is modeled as a quasi-steady process in which the electrochemical-kinetics is assumed to happen at a rate much faster than the transport and heat transfer model dynamics. So, the reactions are assumed to happen instantaneously at the electrolyte surface and to be complete. Diffusion times to the active sites in the electrolyte matrix are also assumed to be the same order as the chemical kinetics and are neglected. With these assumptions, the species consumption and production rates become wholly dependant on the current produced from the cell. At any point in time then, the local current production depends upon local bulk species concentrations in the anode and cathode compartments, an iteratively determined cell voltage (using an electrode equipotential assumption), and the local polarizations. A relatively simple mass/species balance equation for species conservation is thereby obtained [7]:

$$\forall \left(\frac{\mathrm{d}C_k}{\mathrm{d}t}\right) = N_{k,\mathrm{in}} - N_{k,\mathrm{out}} + R_{\mathrm{p}} j \tag{4}$$

where $\forall$ is the finite control volume; C_k, the individual concentration of species k; N_k, the molar flow of species k; R_{p}, the total production rate of species k; and j, the current.

2.1. Cell voltage and loss mechanism

Although the dynamics of the fuel cell in the current model are not impacted by electrochemical dynamics, the impacts of electrochemical dynamics on the realized voltage are well considered and accounted for. The equilibrium cell potential (E_{eq}) of a fuel cell in terms of temperature and gas compositions is given by the Nernst equation [4]:

$$E_{\mathrm{eq}} = E_0 + \frac{R_{\mathrm{u}}T}{2F} \ln\left[\frac{p_{\mathrm{H_2,an}}\, p_{\mathrm{O_2,cat}}^{0.5}}{p_{\mathrm{H_2O,an}}} \frac{p_{\mathrm{CO_2,cat}}}{p_{\mathrm{CO_2,an}}}\right] \tag{5}$$

The Nernst equation provides a relationship between the ideal standard potential (E_0) for the cell reaction and the ideal equilibrium potential for given local temperatures and partial pressures (p_k) of reactants and products. Fuel cell irreversible losses (caused by electrochemical dynamic limitations, as in activation polarization, or by mass transport limitations, or resistive heating) are estimated through local calculation of the three primary bulk losses of activation, concentration, and Ohmic polarizations [4]:

$$V_{\mathrm{cell}} = E_{\mathrm{eq}} - \eta_{\mathrm{act}} - \eta_{\mathrm{conc}} - \eta_{\mathrm{ohm}} \tag{6}$$

where V_{cell} is the cell voltage under load; η_{act}, the activation polarization; η_{conc}, the concentration polarization; and η_{ohm}, the Ohmic polarization. Polarization losses are generally dependent on gas partial pressures, temperature, and current density, all of which are spatially distributed in an actual cell. Several approaches for calculating these polarization losses have been presented in the literature. One approach is to derive the activation polarization and the concentration polarization from the Butler-Volmer equation. Using this approach the activation, concentration and Ohmic polarization equations are, respectively [4]:

$$\eta_{\mathrm{act}} = \frac{R_{\mathrm{u}}T}{\alpha n F} \ln\left[\frac{j}{A j_0}\right] \tag{7}$$

$$\eta_{\mathrm{conc}} = \frac{R_{\mathrm{u}}T}{nF} \ln\left[1 - \frac{j}{A j_{\mathrm{L}}}\right] \tag{8}$$

$$\eta_{\mathrm{ohm}} = j R_{\mathrm{int}} \tag{9}$$

where j_{L} is the limiting current density; j_0, the exchange current density; A, the area of the cell; and R_{int}, the internal resistance

of the fuel cell. The limiting current density is influenced by the transport phenomena that occur in the fuel cell electrodes. The exchange current density is a function of the fuel cell operating pressure and temperature. The work done by Bessette [8], suggests a potential model for j_0 written as ($j_0 = a + bT$), however experimental data indicates that the dependence of j_0 solely on the operating temperature of the cell is insufficient. Previous work done by Rivera [9] shows that the equation ($j_0 = a + bT + cP + dPT$) can be used to predict the value of exchange current density. Values of j_0 across a temperature and pressure range from 590 to 650 °C, 1–3 atm., respectively, vary from 10 to approximately 2500 A m^{-2}. This is within an acceptable range, according to Larminie and Dicks [10]. These values were found by using a value of 0.5 for the transfer coefficient (α).

Another approach is given by Yuh and Selman [1,2], which has received a somewhat general acceptance because it combines a general, macro-homogeneous concept of the active reaction sites (agglomerates) with a specific micro-geometric representation of the gas transport and current conduction in the electrode. In this so-called agglomerate model, the porous electrode is divided spatially into two regions, one consisting of agglomerates of solid particles having liquid-filled micro-pores, and the other consisting of macro-pores. In this approach, the cell potential is calculated by [1,2]:

$$V_{\text{cell}} = E_{\text{eq}} - j(\eta_{\text{an}} - \eta_{\text{cat}} - R_{\text{ohm}}) \tag{10}$$

where E_{eq} is given by Eq. (5). The impedance for anode overpotential (η_{an}) and cathode overpotential (η_{cat}) can then be written as, respectively [1,2]:

$$\eta_{\text{an}} = 2.27 \times 10^{-9} \exp\left(\frac{E_{\text{act,an}}}{R_{\text{u}} T}\right) p_{\text{H}_2}^{-0.42} p_{\text{CO}_2}^{-0.17} p_{\text{H}_2\text{O}}^{-1.0} \tag{11}$$

$$\eta_{\text{cat}} = 7.505 \times 10^{-10} \exp\left(\frac{E_{\text{act,cat}}}{R_{\text{u}} T}\right) p_{\text{O}_2}^{-0.43} p_{\text{CO}_2}^{-0.09} \tag{12}$$

where p_k denotes partial pressure of species k in units of atm.; and E_{act} denotes activation energy. The activation energies used for 650 °C were taken from the work of Yuh and Selman [1,2], while those for other temperatures were extrapolated. The overall cell resistance (electronic and ionic) was expressed with the Arrhenius equation to calculate Ohmic polarization by [11]:

$$R_{\text{ohm}} = 0.45 \times 10^{-5} \exp\left[8600\left(\frac{1}{T} - \frac{1}{923}\right)\right] \tag{13}$$

The pre-exponential factor in Eq. (13) was determined to be 0.45×10^{-5} Ω from measured experimental cell resistance data at 650 °C.

2.2. Energy balance and thermal properties

As mentioned earlier, to perform the energy balance across the cell, each nodal volume was separated into five distinct control volumes: anode and cathode separator plates, anode and cathode channels, and the electrode–electrolyte matrix. These distinct components can be considered individual thermodynamic control volumes, each of which is simulated using a set of dynamic energy and heat transfer equations that account for sources/sinks and interactions between and amongst the components as well as those in adjacent nodes. Within the components, an energy equation was formulated by applying the First Law of Thermodynamics with heat transfer modeled by finite difference methods. To reduce simulation time, the fluid channels were modeled as control volumes with constant properties and a single unique temperature and set of species concentrations. Similarly, the electrolyte was also assumed to have constant properties and was modeled as one bulk component even though it consists of a molten carbonate salt mixture (sodium, potassium, or lithium salts) that is retained in a ceramic matrix of lithium aluminum oxide with electrodes on both sides. For all the solid components, a lumped capacitance condition is assumed.

Due to the cell's planar configuration and operating conditions, the stream-wise and normal to the top of the cell directions were assumed to be the primary directions of heat flux. This is because the largest exposed area is on the upper and lower surfaces of the cell and the thermal profile (due primarily to non-uniform heat generation) and convective fluxes are important in the stream-wise direction.

For the fluid channel, the energy equation is simultaneously solved with the momentum and species conservation equations, which were discussed earlier. For the fluid within the channel flow between the nodes, it was assumed that the mass that leaves or enters the control volume has a specific energy. Thus, an energy balance can determine the bulk fluid temperature within each channel for every node. So, the energy equation can be written as [12]:

$$\not{V}\frac{\mathrm{d}(\rho \mathrm{E})}{\mathrm{d}t} = \sum \mathrm{m}_{\text{in}} \mathrm{E}_{\text{in}} - \sum \mathrm{m}_{\text{out}} \mathrm{E}_{\text{out}} - Q_{\text{conv,e}} - Q_{\text{conv,s}} + E_I \tag{14}$$

where E denotes energy; m is mass flux; Q_{conv}, convective heat transfer in the electrolyte (subscript e) and at the separator plate (subscript s); E_1, the net rate of flow energy added at the control volume inlet and outlet, and the subscripts in and out denote into and out of control volume, respectively.

The separator plates are modeled as uniform-solid components with heat transfer to and from their boundaries. The separator plates have no thermal generation because there is no reaction within the separator plates; but since they are at the edge of the cell, energy can be extracted (lost to the environment from the fuel cell perspective). For the boundary conditions, the separator plates interact with ambient conditions (or neighboring cells if in a stack), with the adjacent fluid channel, and within neighboring separator plate nodes. Applying an energy balance to the separator plates yields the following differential equation [12]:

$$\frac{\mathrm{d}Q}{\mathrm{d}t} = -Q_{\text{cond}_{\text{cs,s}}} - Q_{\text{conv}_{\text{f}}} - Q_{\text{conv}_{\infty}} - Q_{\text{cond}_{\text{cs,s-ele}}} - Q_{\text{ref}} \tag{15}$$

where Q_{cond} denotes conductive heat transfer in the separator plate (subscript s); Q_{conv} is the convective heat transfer in the fluid (subscript f) and to the environment (subscript ∞); and Q_{ref}, the reformer heat exchange losses.

The electrolyte energy equation is similar, however, heat generation terms appear to take into account the formation

of water from the electrochemical conversion of the oxygen and hydrogen gases (Eq. (3)). Heat generation is assumed to occur within the electrode–electrolyte volume. In addition, the boundary conditions differ from the separator plates in that the electrode–electrolyte matrix is surrounded on both top and bottom channels so that only the immediate sides of the cell electrode–electrolyte assembly are able to interact directly with the ambient conditions. The energy equation for the local bulk temperature in the electrode–electrolyte matrix that results is [12]:

$$\frac{\mathrm{d}Q}{\mathrm{d}t} = -Q_{\mathrm{cond_e}} - Q_{\mathrm{conv_{f,an}}} - Q_{\mathrm{conv_{f,cat}}} + Q_{\mathrm{cond_s}} + Q_{\mathrm{gen}} \quad (16)$$

$$Q_{\mathrm{gen}} = j\left(\frac{\Delta H^{\mathrm{f}}_{\mathrm{H_2O}}}{nF} - V_{\mathrm{cell}}\right) \quad (17)$$

The equations used for the conductive and convective heat transfer are of the form, respectively [9]:

$$Q_{\mathrm{cond}} = \frac{kA_{\mathrm{cond}}}{L}\Delta T \quad (18)$$

$$Q_{\mathrm{conv}} = hA_{\mathrm{conv}}\Delta T \quad (19)$$

where A_{conv} is the flux area; k, the thermal conductance of the material the heat flux is going through; L, the distance between the bulk temperature difference; h, the convective heat transfer coefficient; and A_{conv}, the surface area.

3. Discretization

When simulating a fuel cell, it is important to capture some of the geometrical features so that the dynamic performance of cell can be accurately predicted. Even the overall cell performance depends upon local conditions and properties (temperature, pressure, species concentrations) that cannot be accurately captured without some spatial resolution of the mass and heat transfer, chemical and electrochemical reactions as they vary widely throughout the cell or stack volume. In addition, some understanding and insight into local conditions can be valuable for determining whether the fuel cell is subjected to harmful or stressful conditions. However, full three-dimensional and dynamic resolution of the concurrent processes (e.g., chemistry and electrochemistry, heat transfer, mass transfer, momentum) is often computationally intensive. Thus, we have selected an approach that can capture essential spatial features in a relatively simplified manner allowing solution of the dynamic equations that govern heat and mass transfer, momentum and energy conservation, and electrochemistry in the fuel cell.

For simulation, the cell is discretized along the stream-wise direction into 10[1] distinct control volumes in order to capture variations along the length of the cell. Each node is comprised of an identical representation of the five cell components (control volumes) with the exception that the boundary conditions are provided by either adjacent nodes or inlet/exit conditions. The stream-wise discretization allows the model to capture variations along the length of the cell as well as the potential for mass storage during dynamic operation.

The cathode and anode channels are modeled by applying the conservation equations to the nodal control volumes. This allows for the solution of the state variables within the channels. Pressure is obtained by solving the momentum equation, which is an unsteady Bernoulli equation that assumes there is a time-varying, uniform bulk flow. In a separate sensitivity analysis, this Bernoulli equation (which demands a lot of computational time) was solved and solutions compared to the simple assumption of a constant pressure drop (from 1 to 10%). In this analysis, no significant difference in voltage and current was found between the computationally intensive solution of the Bernoulli equation and the assumed pressure drop. As a result, a constant pressure drop (about 0.1% in each node) across the cell was used since the exit pressure is known.

In both channels, mass and species balances are used. Flows are assumed to be ideal gases allowing the inlet concentration to be easily obtained from local pressure and temperature. From inlet flow and molar fractions, the species inlet concentrations can be determined for each node and each control volume. The inlet species concentrations are then used in a mass/species balance with reaction rates to form the relation dictating the exit molar fractions. Due to the Nernst term, there will be a spatial variation in the current generation since the fuel and oxidizer concentrations will decrease along the path of the flow.

Along the length of the cell, a global equal-potential condition is enforced [13]; that is the voltage across the cell throughout all nodes is constant and is also the overall cell voltage. This assumption is reasonable since the current collectors and electrodes in a carbonate fuel cell are relatively good electronic conductors. As a result, at each node the following electrochemical relation applies:

$$V_{\mathrm{cell}} = \sum_{\mathrm{nodes}} j_{\mathrm{node}} R_{\mathrm{load}} \quad (20)$$

Also note that the fuel cell is comprised of a one-dimensional array of nodes and each node is comprised of two-dimensional sets of components (control volumes). This yields an overall two-dimensional cell temperature distribution, which is represented in Fig. 2. Fig. 2 also presents the equivalent circuit heat transfer network of two adjacent nodes showing that the present model accounts for convective and conductive heat transfer between and amongst components as appropriate.

The two models (agglomerate model and simplified model) were developed in MATLAB Simulink® [14], selected because of dynamic solution capabilities, a flexible and versatile user interface, and especially, compatibility with dynamic control system development. The models are constructed in a physically representative manner, i.e., separate graphical components representing the anode, cathode, electrode–electrolyte assembly, etc., for each of the model nodes, allowing easy visualization and debugging. The two models are constructed similarly using the

[1] As stated before, a node sensitivity analysis showed that, in this case, the fuel cell model needed to be divided into 10 nodes in order to achieve high accuracy. Using more than 10 nodes only provides small gains in accuracy with a large increase in computation time [7,9].

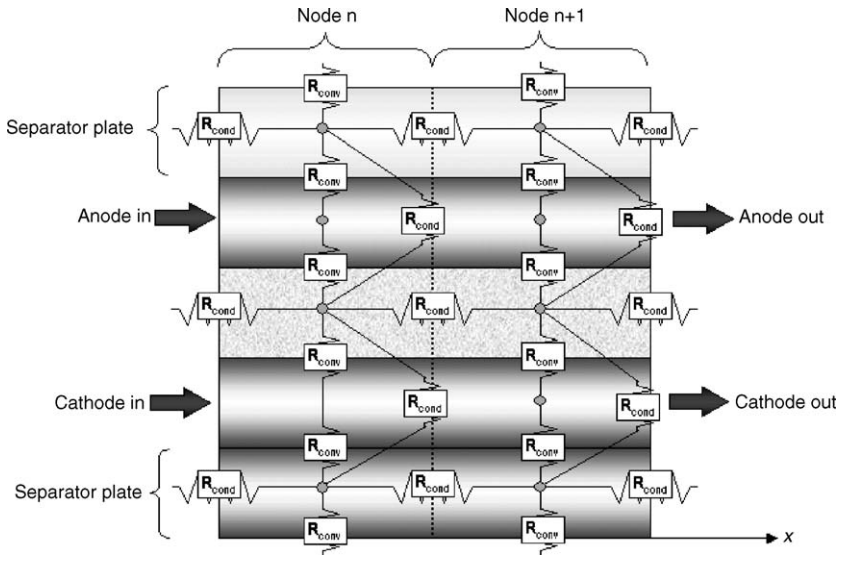

Fig. 2. Schematic representation of heat transfer at the nodal level [13].

same energy conservation equations; they differ only in the manner in which electrochemical and transport losses are calculated in each node.

4. Experimental investigation

An experimental investigation was conducted to measure the performance of a single MCFC cell. The experiments were designed to acquire data that could be useful for model validation. The MCFC tested has a planar area of 100 cm^2. The test stand used sandwiched the actual cell between separator plates that were machined with 21 channels mat are 3 mm in width and height for the cathode and 3 mm in width and 1.5 mm in height for the anode. This contributes to a relatively simple and yet still complex geometry for the solution of mass and heat transfer equations. The electrode–electrolyte matrix is sandwiched between the two opposing separator plates and the fuel and oxidant flow concurrently in opposing channels.

A total cross-sectional area is calculated using actual cell geometry but features such as defects in the structural interconnections within the electrode–electrolyte structure itself and to the separator plates are ignored. The separator plates are modeled in a similar fashion as the electrolyte; as constant property flat plates that have no complex features with a cross-sectional area that is the same as the actual cell. For model validation, only 5 species are simulated in the anode and cathode channels: CO_2, H_2, H_2O, N_2, and O_2 since these were the only gases used and measured in the experiments. Electric heaters were used to heat the fuel cell to a specified temperature because, unlike a fuel cell stack, a single cell is not capable of producing the heat necessary for self-sustained operation.

The internal resistance of the cell was measured at different temperatures and pressures. The procedure consists of generating an almost instantaneous change of the cell load current and observing the voltage response. Using an oscilloscope the difference in cell voltage was measured. This difference was then divided by the difference in current to give the internal resistance. These measured internal resistance values were directly used to calculate Ohmic polarization in the model [9].

5. Results and discussion

The fuel cell parameters and operating conditions employed for the simulation are shown in Table 1. Table 2 presents the heat

Table 1
Unit cell data and operating conditions for the MCFC dynamic model

Parameter	Value
Load resistance (Ω)	0.0692
Number of channels	21
Operating pressure (Pa)	101,325–303,975
Operating temperature (K)	860–923
Limiting current density (A m^{-2})	4000
Transfer coefficient	0.5
Cell thickness (m)	0.01
Separator plate thickness (m)	0.0017
Separator plate density (kg m^{-3})	7900
Separator plate heat capacity (J kg^{-1} K^{-1})	611
Electrolyte thickness (m)	0.001
Activation energy in the anode (kJ $kmol^{-1}$)	53,500
Activation energy in the cathode (P = 101,325 Pa) (kJ $kmol^{-1}$)	102,800
Activation energy in the cathode (P = 202,650 Pa) (kJ $kmol^{-1}$)	99,000
Activation energy in the cathode (P = 303,975 Pa) (kJ $kmol^{-1}$)	93,000
Inlet molar fraction of H_2 in the anode	0.60
Inlet molar fraction of CO_2 in the anode	0.15
Inlet molar fraction of H_2O in the anode	0.25
Inlet molar fraction of O_2 in the cathode	0.08
Inlet molar fraction of N_2 in the cathode	0.59
Inlet molar fraction of CO_2 in the cathode	0.08
Inlet molar fraction of H_2O in the cathode	0.25

Table 2
Parameters for the heat transfer equations in the model

Conduction	h ($Wm^{-2}K^{-1}$)	A (m^2)	L (m)
Separator plate to separator plate (cathode)	25.4	0.000214	0.01
Separator plate to separator plate (anode)	25.4	0.000147	0.01
Separator plate to electrolyte (cathode)	25.4	0.000357	0.0031
Separator plate to electrolyte (anode)	25.4	0.000357	0.0013
Electrolyte to electrolyte	218	0.0001	0.01

Convection	h ($Wm^{-2}K^{-1}$)	A (m^2)
Separator plate to anode gas	83.86	0.0012
Separator plate to cathode gas	92.96	0.0020
Separator plate to ambient air		
Top and bottom	10.00	0.0010
Sides	10.00	0.0005
Electrolyte to ambient air	21.00	0.0001

transfer coefficients and areas used in the model for the energy equations.

The results are showed for the agglomerate model and simplified model. The agglomerate model uses Eqs. (4), (5) and (9)–(13), while the simplified model uses Eqs. (4)–(9). All other equations are identical in both models.

Both the experiments and the simulations were carried out for a set of overall pressure and temperature conditions, with pressure ranging from 1 to 3 atm., and with overall temperatures of 590, 620, and 650 °C. The results showed are only for the worst case (590 °C) and the best case (650 °C) cell performance conditions.

5.1. Steady-state performance comparison

The polarization curves represent the voltage-current characteristics of the electrochemical reaction that occurs inside the fuel cell. The measured and predicted current-voltage curves are shown in Figs. 3 and 4 for the temperatures of 590 and 650 °C, respectively. These figures show results from the models as well as those obtained experimentally for three overall operating pressure conditions (1, 2, and 3 atm.). These plots show primarily the kinetically dominated region for the MCFC (low current density).

The results exhibited in Fig. 3 (590 °C cases) show a maximum deviation in voltage between experiment and model of about 3% for the agglomerate model and of about 9% for the simplified model. The maximum covariance[2] for the agglomerate model is about 3%, and for the simplified model about 22% relative to the experimental results.

The results displayed in Fig. 4 (650 °C cases) show a maximum deviation of only about 1.5% for the agglomerate model while the simplified model shows a maximum deviation in voltage of 3%. In this set of values, the maximum covariance for the agglomerate model is about 0.4%, and that of the simplified model is about 1.8% related to the experimental results.

This comparison of cell current-voltage performance is very good and well verifies the steady-state model convergence to a reasonable solution. The comparisons shown in Fig. 4 for both the agglomerate and simplified models are in especially good agreement with experimental data. In all cases, the agglomerate model can be used to obtain more accurate results. The simplified model can predict the steady-state performance of the fuel cell with larger error, yet it uses only overall pressure and temperature to determine the electrochemical losses. If the relatively larger error of the simplified model is acceptable, then

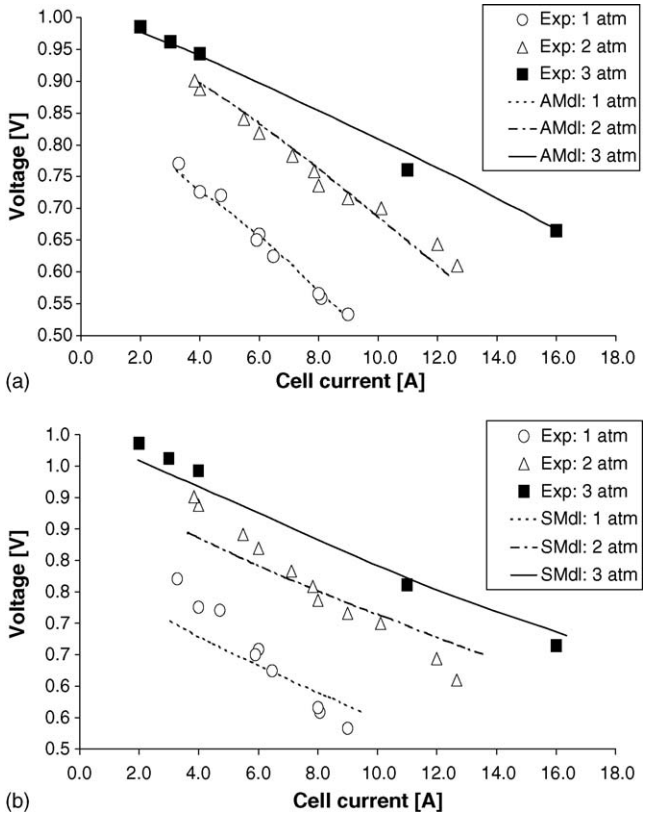

Fig. 3. Voltage vs. current for the experimental, agglomerate model (a); and simplified model (b) results for 590 °C.

[2] The maximum statistical measure of correlation of the fluctuations of two data sets (experimental versus model).

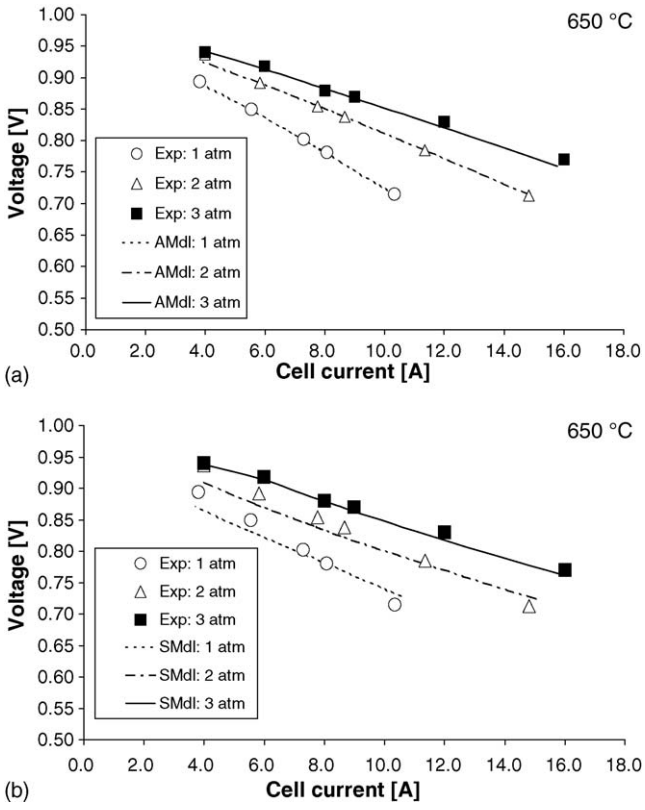

Fig. 4. Voltage vs. current for the experimental, agglomerate model (a); and simplified model (b) results for 650 °C.

one can use this simplified model with parameter requirements (e.g., overall temperature and pressure) that can be much more easily obtained and measured for verification and calibration.

5.2. Dynamic performance comparison

Generally, when a fuel cell experiences a load change it responds with a quick electrochemical and transport transient and a slower thermal response. Since most of the physical and chemical processes that govern fuel cell operation are strongly temperature dependent, the thermal transient affects cell voltage and current as well. In a typical system, these thermal transients can have long time constants (e.g., 100's to 1000's of seconds) due to the relatively large thermal mass of a fuel cell. In the current experiment, however, care was taken to control (and monitor) temperature within a narrow window of operation for all the results presented herein. This was accomplished with controllable heaters, thermocouples, and insulating materials that surrounded the fuel cell during the tests. Thus, the dynamic response of interest in the current study is one that accounts primarily for the electrochemical and transport controlled dynamics together with the small amount of more immediate temperature variations that occur along the length of the cell and for the cell overall.

The dynamic response of the MCFC cell was measured in the experiments for step changes in applied load resistance. Identical step changes in load resistance were applied in the simulations. In the simulations, the load of the cell was decreased from 0.1533 to 0.0692 Ω, representing a decrease of about 55%, in order to determine the dynamic response of fuel cell voltage and current.

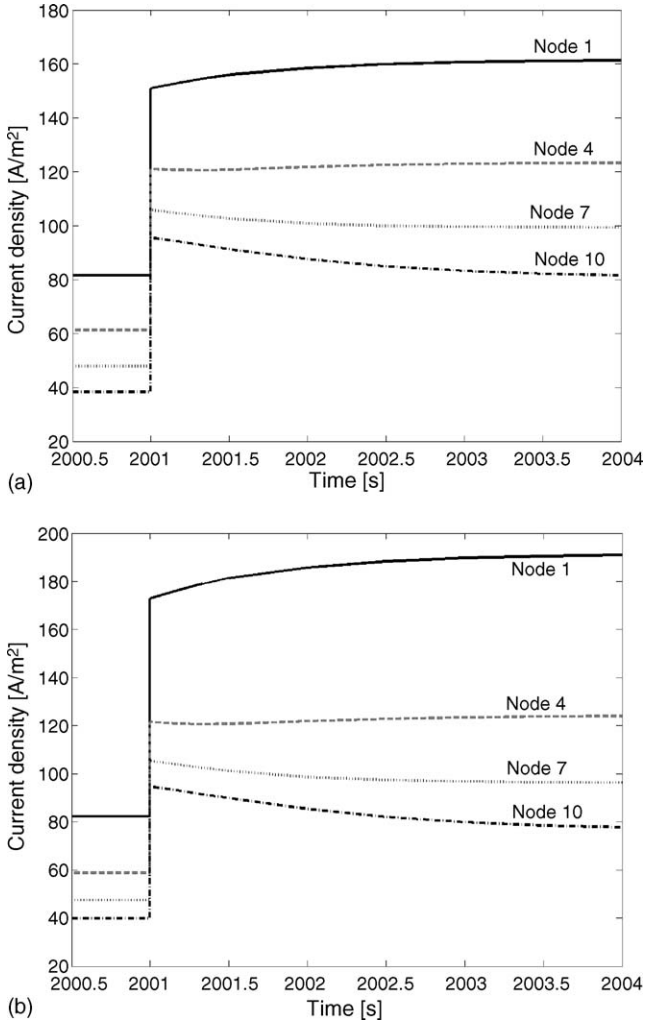

Fig. 5. Results of dynamic response of cell current density during load resistance decrease (650 °C and 2 atm.): (a) agglomerate model; and (b) simplified model.

The behaviour of current density along the length of the cell was investigated leading to similar current density profiles for operating temperature conditions of 590 and 650 °C. Fig. 5 displays the distribution in current density of both models for the case when the overall cell temperature was 650 °C. In this figure, for time <2000 s, the cell current density corresponds to the steady-state value for the initial load resistance. The asymptotic value for time >2010 s corresponds to the new steady-state current density distribution. The intermediate period shows a fast initial increase in all nodal current levels (minimum of about 85% for the agglomerate model and about 110% for the simplified model), a subsequent smaller increase for upstream nodes over time, and a subsequent decrease for the downstream nodes over time. In the agglomerate model (Fig. 5a), the increase was of about 11% for the first node and the decrease of about 17% for the tenth node in this intermediate time frame. For the simplified model (Fig. 5b) the increase was of about 16% for the first node and the decrease of about 20% for the tenth node in this intermediate timeframe. The transient behaviour is due to

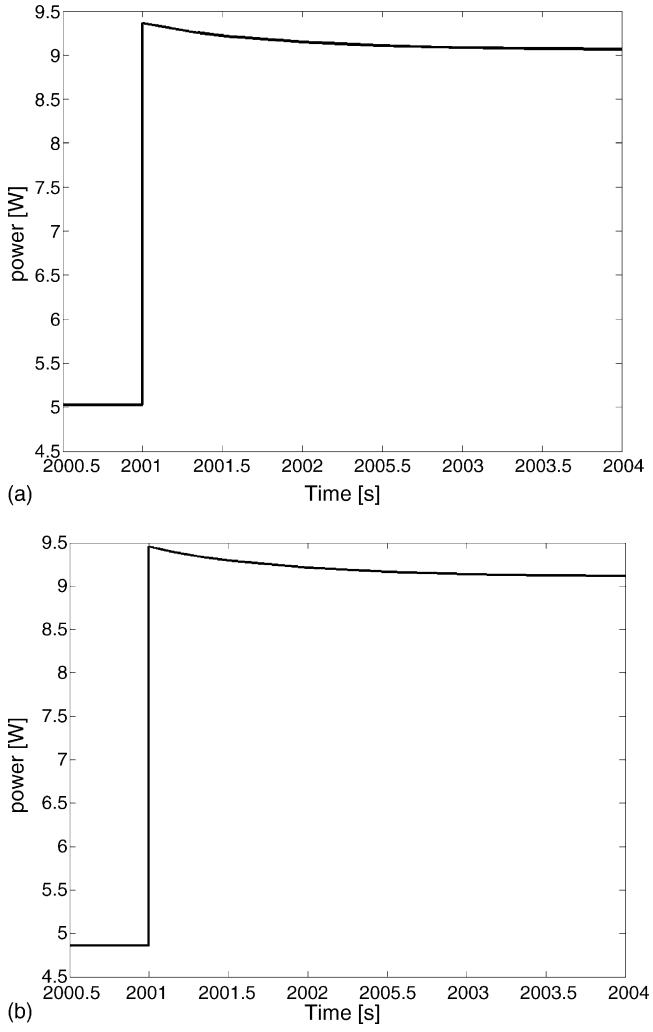

Fig. 6. Effect of load change on a cell power (650 °C and 2 atm.) using: (a) agglomerate model; and (b) simplified model.

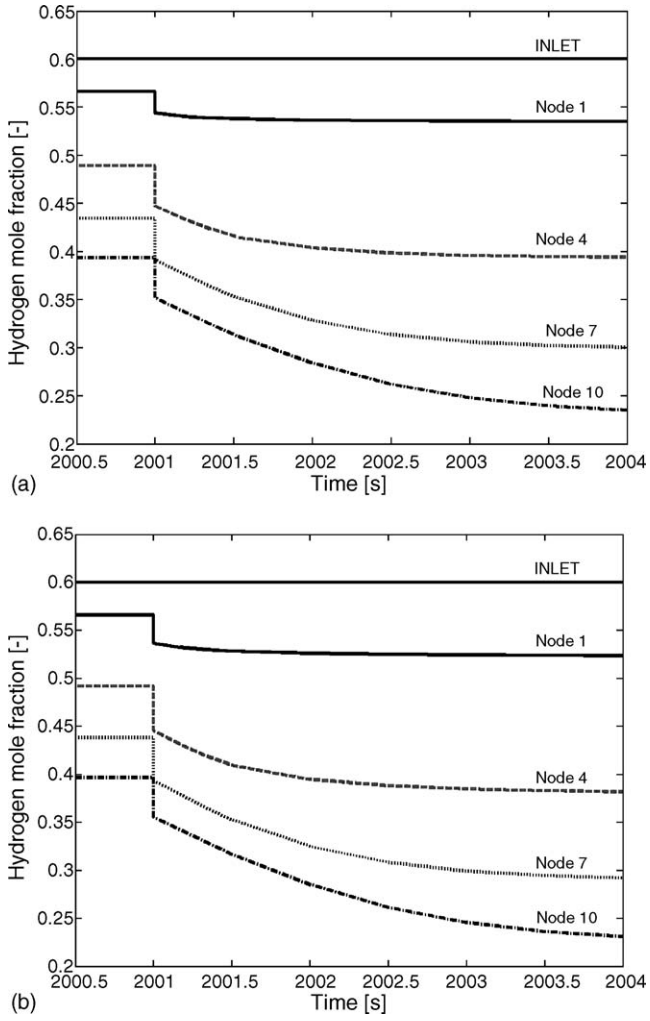

Fig. 7. Transient hydrogen mole fraction during 55% load resistance: (a) agglomerate model; and (b) simplified model.

the readjustment of the electrochemistry, and material residence response times. If one assumed a uniform current density unrealistic higher voltages would result upstream due to the gradient in hydrogen concentration in the stream-wise direction. However, the current collectors (electrodes) more realistically are at the same voltage (as indicated by Eq. (20)), which results in a higher current density upstream (creating higher local losses) that must settle to achieve a uniform voltage to satisfy Eq. (20). In this case, the Nernst potential has to be iteratively readjusted inside each node of the model for each time-step. This spatially uniform voltage and spatially varying current behavior is qualitatively similar to that observed in experiments reported by Mench et al. [15] and Mench and Wang [16].

Fig. 6 presents the transient response of fuel cell power, which is voltage times current, to the decreased load resistance perturbation under 650 °C operating conditions. For the agglomerate model (Fig. 6a), the initial power increases from 5.027 to 9.367 W, representing an increase of about 86%. This is followed by a gradual decrease in power to approximately 9.267 W over a time period of about 50 s (only the first 4 s of the transient are shown). This new steady-state condition corresponds to an overall power increase of about 84%. When using the simplified model (Fig. 6b), the initial power increases from 4.860 to 9.454 W, representing a slightly larger initial increase than that observed with the agglomerate model, i.e., of about 95%. This is followed by a gradual decrease in power to approximately 9.280 W (overall increase of about 91%) over a time period of about 30 s (only the first 4 s of the transient are shown). Comparing the two models, the simplified model provided an initial lower steady-state voltage, but higher percentage difference in the initial transient. Given the available reactant concentration in cell, when the load resistance decreases the cell readjusts to get more current at the same voltage. Thus, the curves resulting from both of the models present a peak in power in the instant just after the change in load. As the reactants are consumed, the Nernst term reduces voltage and forces the readjustment of overall current distribution to a higher current and lower voltage. Note that the overall resulting increase in power is similar for both models.

Fig. 7 shows the results for the hydrogen mole fraction in the anode gas stream versus time for several of the individual model nodes for the 650 °C case using both models. As is seen in Fig. 7,

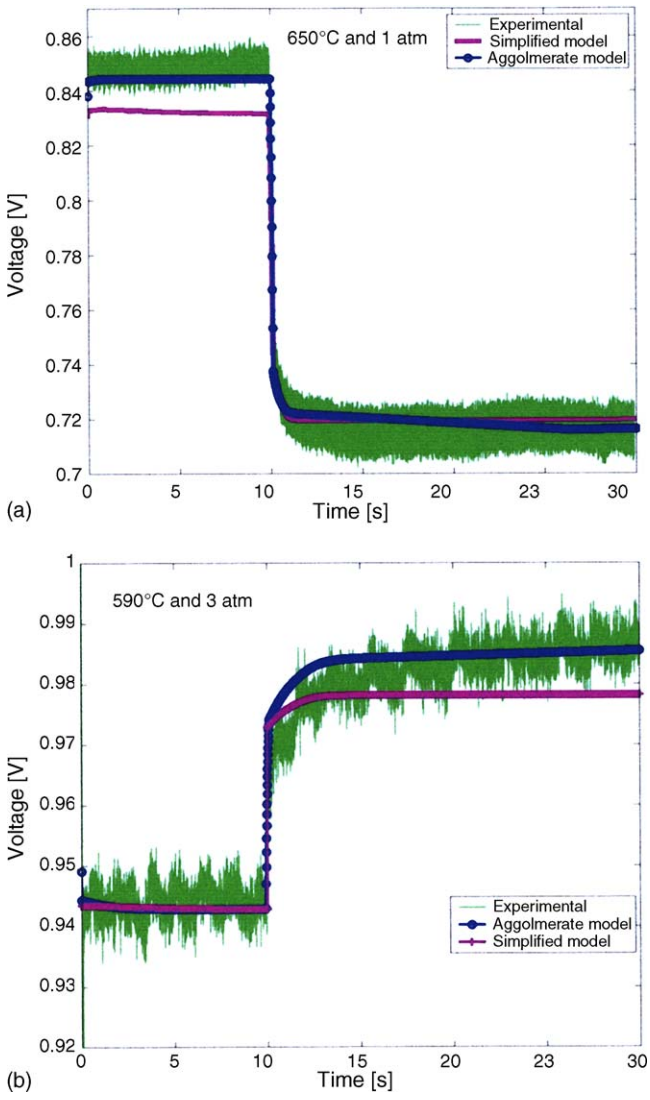

Fig. 8. Experimental, agglomerate model and simplified model results of dynamic voltage response for: (a) 650 °C, 1 atm. and 55% load decrease; and (b) 590 °C, 3 atm. and 52% of load increase.

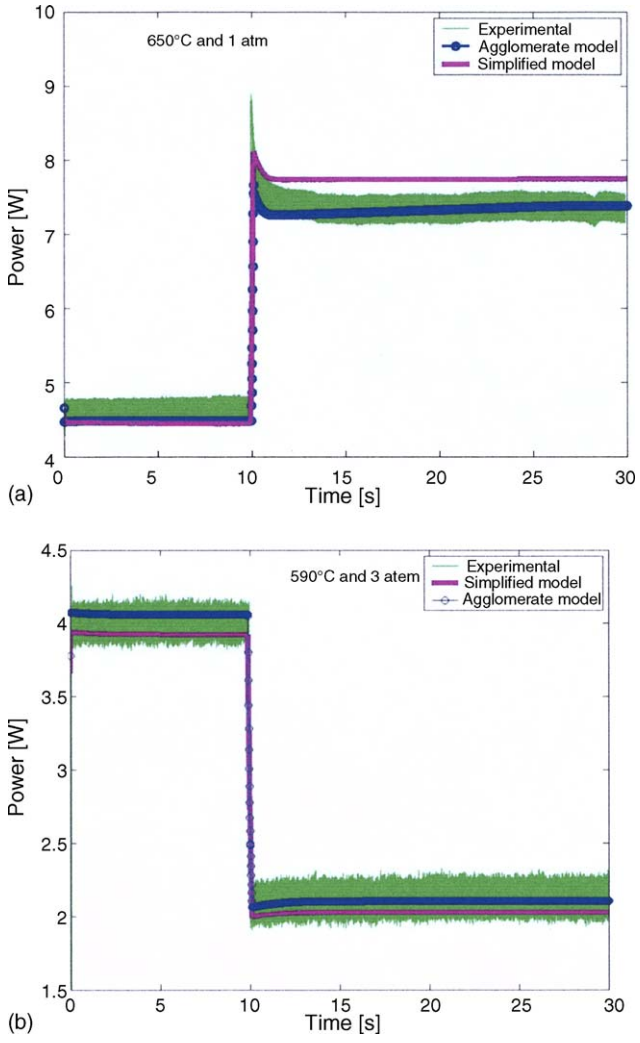

Fig. 9. Experimental, agglomerate model and simplified model results of dynamic power response for: (a) 650 °C, 1 atm. and 55% load decrease; and (b) 590 °C, 3 atm. and 52% of load increase.

the upstream nodes have a relatively small H_2 concentration transient response. Downstream nodes, however, exhibit a change in H_2 concentration that results from the cumulative response of all upstream nodal H_2 consumption increases as indicated by the differences from node 1 to node 10. The two models are similar in their predicted transient response of hydrogen concentration to the load perturbation in both space and time.

Fig. 8a shows a comparison of the fuel cell voltage dynamic response to a perturbation in the applied load resistance. The perturbation applied in both the experiment and in the models corresponds to a 55% load resistance decrease, i.e., from 0.1533 to 0.0692 Ω, an overall temperature condition of 650 °C and a pressure of 1 atm. The results show that both of the models can well predict the dynamic response of the fuel cell. The comparison proves that predictions are within an expectable level of accuracy for a significant load decrease. Both the transient response time (about 5 s) and initial and final voltages are well predicted by the models. The second curve (Fig. 8b) shows the results for a 52% load resistance increase (from 0.2375 to 0.4900 Ω), with an overall temperature condition of 590 °C and a pressure of 3 atm. These results also show that predictions are within an expectable level of accuracy.

Fig. 9 displays the results of dynamic power response for the same perturbation and operating conditions as those presented in Fig. 8. The results show that the agglomerate model provides better correspondence to measurements for both temperatures. These results are in accordance with those presented in Fig. 6. In the experimental set-up only voltage and current were measured. Thus, the discrepancies between model and experiment may be partially attributable to the measurement strategy. The results in power, especially the ones showed in Fig. 9a, display an exaggerated peak in power that is a result of multiplying two noisy data streams (voltage and current). Except for this discrepancy, the transient response of the data is fairly well predicted by both models, which predict a peak in power as expected since the load resistance was decreased (power demand was increased). For the case when the perturbation was a decrease in power demand at overall 590 °C and 3 atm. conditions Fig. 9b demon-

strates a predicted slight undershoot when the load is increased, which is also exhibited in the models.

6. Summary and conclusions

Understanding of fuel cell performance can be obtained by experimental measurements and/or theoretical modeling. Experimental investigation is a time-consuming and expensive process, while theoretical modeling is relatively fast and inexpensive. However, theoretical modeling usually requires experimental validation in order to be considered a viable alternative to measurements. The dynamic operation of systems based on fuel cell technology are complex and include, for example, the interaction between electrochemical, physical, chemical, and thermal (heat transfer) processes. As a result, accurate and high fidelity models that can capture the dynamic behavior of the fuel cell and identify the thermal gradients within the cell are desired.

In this work, a detailed model was developed in the MATLAB Simulink® environment using the principles of fluid dynamics, electrochemical and chemical reaction mechanisms, and heat-transfer that govern a MCFC. A two-dimensional geometric representation of the cell is included. The model was applied to predict dynamic variations of voltage, current and power in an MCFC as it responds to varying load demands.

A corresponding set of experiments were carried out for a single MCFC cell using a test stand that can apply perturbations and measure the cell performance for a set of otherwise fixed operating conditions. The experiments were conducted at various overall temperature (590–650 °C) and pressure conditions (1–3 atm.) in a manner to allow direct comparison to the dynamic simulation results. A series of simulations and analyses were carried out to verify model performance. The models are shown to provide simulation results that are in good agreement with experimental results.

The results for steady-state performance comparison demonstrated that a simplified model can be used to get a reasonable solution of current-voltage characteristics while the agglomerate model can be used to get more accurate results. The results of dynamic performance comparisons showed the effect of a load decrease on the local (spatially resolved) cell current, hydrogen usage and power predicted by two models. The models revealed the dynamic response of current density along the cell length with a fast initial increase in all nodes, a subsequent smaller increase for upstream nodes and decrease for downstream nodes in the immediate aftermath of the perturbation.

The results in current density are related to the results of hydrogen mole fraction, which indicated that the overall cell voltage results from a cumulative response of upstream nodes that determines the cell hydrogen concentration profile in response to the perturbation. The results of predicted dynamic voltage response characteristics of both models for various overall temperature and pressure operating conditions compared well with observed dynamic responses. The presented transient responses of the fuel cell voltage to increasing and decreasing load perturbations provide valuable insight into the operating characteristics of an MCFC for various overall temperature and pressure conditions. Also, the power dynamic responses for a load decrease and load increase were observed with both models predicting the dynamic power response behavior of the fuel cell within an expectable level of accuracy.

These analyses demonstrate that first principles simulation using simplified cell geometry can be useful for garnering insight into the dynamic response characteristics and behavior of fuel cells. Future use of such verified simple models may be especially valuable in detailed system simulations.

Acknowledgements

We gratefully acknowledge the support of the California Energy Commission, which partially supported the development of a dynamic MCFC model.

We acknowledge the support of the National Energy Technology Laboratory, which donated the test stand used in the experiments and contributed to the model development.

We are also grateful for the financial support provided by CNPq (Conselho Nacional de Desenvolvimento Científico e Tecnológico, Brasil, processo 200979/2003–5) to Elisângela Leal.

References

[1] C.Y. Yuh, J.R. Selman, The polarization of molten carbonate fuel cell electrodes: I. Analysis of steady state polarization data, J. Electrochem. Soc. 138 (1991) 3642–3648.
[2] C.Y. Yuh, J.R. Selman, The polarization of molten carbonate fuel cell electrodes: II. Characterization by AC impedance and response to current interruption, J. Electrochem. Soc. 138 (1991) 3649–3655.
[3] A.J. Appleby, in: L.J.M.J. Blomen, M.N. Mugerwa (Eds.), Fuel Cell Systems, Plenum Press, New York, 1993, pp. 157–197.
[4] EG&G Technical Services Inc., Science Applications International Corporation, Fuel Cell Handbook, sixth ed., Under Contract No. DE-AM26-99FT40575, U.S. Department of Energy, Office of Fossil Energy, NETL, November 2002.
[5] FuelCell, Energy Corporation (http://www.fce.com/), 2004.
[6] R.S. Gemmen, E.A. Liese, J.G. Rivera, F. Jabbari, J. Brouwer, Development of dynamic modeling tools for solid oxide and molten carbonate hybrid fuel cell gas turbine systems, in: 2000 ASME Turbo Expo, International Gas Turbine Institute, Munich, Germany.
[7] E.A. Liese, R.S. Gemmen, F. Jabbari, J. Brouwer, Technical development issues and dynamic modeling of gas turbine and fuel cell hybrid systems, in: 1999 ASME Turbo Expo, International Gas Turbine Institute, Indianapolis, June 1999.
[8] N.F. Bessette, Modeling and Simulation for Solid Oxide Fuel Cell Power Systems, Ph.D. Dissertation, Georgia Institute of Technology, 1994, 212 pp.
[9] J.G. Rivera, Establishment of a predictable mathematical model for a molten carbonate fuel cell, Thesis, M.Sc. in Engineering, University of California, Irvine, 2000.
[10] J. Larminie, A. Dicks, Fuel Cell Systems Explained, John Wiley & Sons Ltd, New York, NY, 2000.
[11] J.H. Koh, B.S. Kang, H.C. Lim, Analysis of temperature and pressure fields in molten carbonate fuel cell stacks, AIChE J. 47 (9) (2001) 1941–1956.
[12] E. Achenbach, Three-dimensional and time-dependent simulation of a planar solid oxide fuel cell stack, J. Power Sources 49 (1994) 333–348.

[13] R.A. Roberts, F. Jabbari, J. Brouwer, G.S. Samuelsen, E.A. Liese, R.S. Gemmen,. Inter-laboratory dynamic modeling of a carbonate fuel cell for hybrid application, in: International Gas Turbine Institute Meeting of the ASME, Atlanta, Georgia, 16–19 June 2003.

[14] Simulink/MATLAB is a product of The Mathworks, 3 Apple Hill Drive, Natick, MA 01760-2098, USA (http://www.mathworks.com/).

[15] M.M. Mench, C.Y. Wang, M. Ishikawa, In situ current distribution measurements in polymer electrolyte fuel cells, J. Electrochem. Soc. 150 (8) (2003) A1052–A1059.

[16] M.M. Mench, C.Y. Wang, An in situ method for determination of current distribution in PEM fuel cells applied to a direct methanol fuel cell, J. Electrochem. Soc. 150 (1) (2003) A79–A85.